Spectroscopy of Tb^{3+} ions in monoclinic $KLu(WO_4)_2$ crystal: Application of an intermediate configuration interaction theory

Pavel Loiko[1], Anna Volokitina[1], Xavier Mateos[2,*], Elena Dunina[3], Alexey Kornienko[3], Elena Vilejshikova[4], Magdalena Aguiló[2] and Francesc Díaz[2]

[1]*ITMO University, Kronverkskiy Pr., 49, 197101 Saint-Petersburg, Russia*
[2]*Física i Cristal·lografia de Materials i Nanomaterials (FiCMA-FiCNA)-EMaS, Dept. Química Física i Inòrganica, Universitat Rovira i Virgili (URV), Campus Sescelades, E-43007 Tarragona, Spain*
[3]*Vitebsk State Technological University, 72 Moskovskaya Ave., 210035 Vitebsk, Belarus*
[4]*Center for Optical Materials and Technologies (COMT), Belarusian National Technical University, 65/17 Nezavisimosti Ave., 220013 Minsk, Belarus*

*Corresponding author, e-mail: xavier.mateos@urv.cat

Abstract The spectroscopic properties of Tb^{3+} ions in monoclinic $KLu(WO_4)_2$ double tungstate crystal are studied with polarized light. The absorption spectra in the visible, near- and mid-IR including the transitions to all lower-lying ^7F_J (J = 0...5) excited states are measured. The maximum absorption cross-section for the $^7F_6 \rightarrow {}^5D_4$ transition is 3.42×10^{-21} cm^2 at 486.7 nm for light polarization $\boldsymbol{E} \parallel N_m$. The transition probabilities for Tb^{3+} ions are calculated within the Judd-Ofelt theory modified for the case of an intermediate configuration interaction (ICI). The radiative lifetime of the $^5D_4$ state is 450 μs and the luminescence quantum yield is >90%. The polarized stimulated-emission cross-section spectra for all $^5D_4 \rightarrow {}^7F_J$ (J = 0...6) emission channels are evaluated. The maximum σ_{SE} is 11.4×10^{-21} cm^2 at 549.4 nm (for $\boldsymbol{E} \parallel N_m$). Tb^{3+}:$KLu(WO_4)_2$ features high transition cross-sections for polarized light being promising for color-tunable visible lasers and imaging.

Keywords: double tungstates; terbium ions; absorption; luminescence; Judd-Ofelt theory; stimulated emission.

1. Introduction

Among the trivalent rare-earth ions (RE^{3+}), Sm^{3+}, Eu^{3+}, Tb^{3+} and Dy^{3+} are rather attractive for obtaining multi-color laser emission in the visible [1]. In particular, the Tb^{3+} ions (electronic configuration: [Xe]$4f^8$) are featuring a higher-lying (energy: ~20500 cm^{-1}) metastable excited state ($^5D_4$) and a set of lower-lying ^7F_J states (J = 6...0 in order of increasing energy) [2]. This leads to multiple visible emissions due to the $^5D_4 \rightarrow {}^7F_J$ transitions that fall into the blue, green, yellow and red spectral ranges [3]. The $^5D_4$ state is long-living (from hundreds of μs to few ms) [3] and the corresponding luminescence quantum yield can be high due to the weak non-radiative (NR) processes even in oxide matrices with high phonon energies. The $^5D_4 \rightarrow {}^7F_5$ transition at ~545 nm is the most probable one and a purely green emission from Tb^{3+} has been observed [4]. The rich structure of higher-lying excited-states of Tb^{3+} allows for efficient UV excitation of these ions.

Aside from the interest to Tb lasers, there are multiple studies of Tb^{3+}-based green phosphors based on various matrices, i.e., glasses, glass-ceramics and nanoparticles [5-10]. This extended the understanding of Tb^{3+} spectroscopy. In recent years, the main interest shifted towards (Eu^{3+}, Tb^{3+}) and (Yb^{3+}, Tb^{3+}) codoped materials. The former codoping scheme brings the advantage of continuous color tuning (from red for singly Eu^{3+} doping to green for the Tb^{3+} one) [11,12]. The second codoped system is promising for down-conversion (DC) suitable to enhance the efficiency of silicon solar cells [13,14]. Such DC materials provide emission of up to 2 near-IR (~1 μm) photons from Yb^{3+} ions after the absorption of a single UV photon by a Tb^{3+} ion [13].

There are several early reports about the stimulated-emission from a Tb^{3+}-doped glass [15], an organic solution [16] and a Tb:$LiYF_4$ crystal [17] under broadband flashlamp-pumping, and from a Tb^{3+}-doped fiber laser [18]. Recently, efficient room-temperature (RT) Tb lasers were demonstrated using various fluoride crystals, namely $LiYF_4$, $LiLuF_4$, KY_3F_{10}, BaY_2F_8, CaF_2, LaF_3 and TbF_3 [3,19]. Lasing at ~545 nm (in the green, $^5D_4 \rightarrow {}^7F_5$ transition) and at ~585 nm (in the yellow, $^5D_4 \rightarrow {}^7F_4$ transition) were achieved. In the study of Metz *et al.*, a highly-doped (28 at.%) Tb:$LiLuF_4$ laser pumped by a frequency-doubled optically pumped semiconductor laser (2ω-OPSL) at 486 nm (to the $^5D_4$ state) generated a maximum green output power of 1.13 W with a slope efficiency of 52% with respect to the absorbed pump power. In [19], wavelength tuning of Tb:CaF_2 and Tb:$LiLuF_4$ lasers between ~540 and 550 nm was also demonstrated.

The physical reason for application of fluoride crystals in Tb lasers is the following. Among the RE^{3+} ions, Tb^{3+} has one of the lowest energy separations between the multiplets of the $4f^8$ configuration and the $4f^85d^1$ excited one [20]. The $4f^8 \rightarrow 4f^85d^1$ transitions (e.g., the excited-state absorption (ESA)) are parity-allowed and thus more intense than the $4f^8 \rightarrow 4f^8$ transitions. Such interconfigurational ESA can strongly affect the laser performance [1,3]. For fluoride crystals, the so-called crystal field depression (CFD, which determines the splitting of the $4f^85d^1$ levels and depends strongly on the host material) is small [20]. Thus, the unwanted interactions with the excited configuration are diminished. However, as it was shown by Metz *et al.*, different host materials even with high CFD (e.g., oxide crystals) can be potentially suitable for Tb lasers.

Among the oxide crystals, the monoclinic double tungstates (MDTs) having a chemical formula of $KRE(WO_4)_2$ (shortly KREW) where RE stands for Y, Gd, Lu or Yb, are very attractive for RE^{3+} doping [21]. The two main features of MDTs are the high transition cross-sections

for polarized light and high available RE^{3+} doping levels accompanied by weak luminescence quenching. Besides the ions suitable for near-IR lasers (at ~1 μm and at ~2 μm) [21], MDTs are recognized to be promising for visible lasers [22,23]. Dashkevich *et al*. presented a RT Eu:KGdW laser operating at 702 nm [23]. Stimulated-emission of Dy^{3+} ions in KYW (at 574 nm and 664 nm) was observed by Kaminskii *et al*. [24] at low temperature. Concerning Tb^{3+}-doped MDTs, very scarce data can be found in the literature. The previous work on Tb:KLuW focused only on the crystal growth and thermal properties [25]. In Refs. [26-28], the luminescence of Tb^{3+} ions in isostructural KYW and KYbW crystals was studied. In particular, Loiko *et al*. reported on the polarized spectroscopy of Tb^{3+} ions in KYbW [28]. However, this is a stoichiometric crystal and it is less attractive for laser applications due to the possible $Yb^{3+} \leftrightarrow Tb^{3+}$ energy-transfer processes.

The aim of the present work is to study the optical absorption and emission of Tb^{3+} ions in the monoclinic KLuW crystal with polarized light and to calculate the Tb^{3+} transition probabilities using the modified Judd-Ofelt theory.

2. Crystal growth

The KLuW crystal doped with 3 at.% Tb^{3+} (N_{Tb} = 1.93×10^{-20} cm^{-3}, crystal density, ρ = 7.613 g/cm^3) was grown by the Top Seeded Solution Growth (TSSG) Slow-Cooling method using potassium ditungstate, $K_2W_2O_7$, as a solvent, see more details in Ref. [21]. The starting materials, K_2CO_3, Lu_2O_3, Tb_2O_3 and WO_3, were from Aldrich and Fluka (>99.9% purity). A seed from an undoped KYW crystal was used for starting the nucleation and was oriented along the [010] crystallographic axis. The structure of the grown crystal was confirmed with X-ray powder diffraction. Tb:KLuW is monoclinic (space group C^6_{2h} – *C2/c*, No. 15, point group: 2/*m*). The as-grown crystal was transparent, it was free of cracks and inclusions. The crystal had a slight yellow-brown coloration due to the Tb^{3+} ions.

3. Experimental

The MDT crystals, including Tb:KLuW, are optically biaxial and have three principal refractive indices, $n_p < n_m < n_g$ [21]. The spectroscopic properties are then characterized in the frame of the optical indicatrix, with the three orthogonal axes, denoted as N_p, N_m and N_g, respectively. For all monoclinic crystals, one of the optical indicatrix axes (it is N_p for MDTs) is parallel to the C_2 symmetry axis (or ***b*** crystallographic one). The two remaining optical indicatrix axes are located in the orthogonal mirror plane (the ***a-c*** plane). For KLuW, the angles N_m^a = 59.3° and N_g^c = 18.5° [21].

For the spectroscopic studies, we cut and polished a parallelepiped sample from the 3 at.% Tb:KLuW crystal with thicknesses t of 4.25 mm and 5.00 mm along the N_g- and N_p-axes, respectively, and thus giving access to all three principal polarizations.

The RT (293 K) absorption spectrum in the visible (0.36-0.51 μm) was measured with a Varian CARY-5000 spectrophotometer (Agilent). The spectral bandwidth (SBW) was 0.01 nm. The absorption cross-section was calculated from the absorption coefficient, $\sigma_{abs} = \alpha/N_{Tb}$. The RT absorption spectrum in the near-IR (1800-6200 cm^{-1}) was measured using a FTIR spectrometer

Bruker Tensor 27 with a spectral resolution of 1 cm^{-1}. The spectra were measured for polarized light using a Glan-Taylor polarizer.

The polarized RT emission spectra of Tb:KLuW were measured with a Renishaw inVia confocal micro-Raman microscope with a x50 objective and an 1800 l/mm grating. The excitation wavelength λ_{exc} was 458 nm or 488 nm. The spectra were combined to cover the 0.48-0.7 μm spectral range. The spectral resolution was ~1 cm^{-1}.

For the RT luminescence decay studies, a Cary Eclipse fluorescence spectrometer (Agilent) was used. The excitation wavelength λ_{exc} was 365, 380 or 475 nm. The decay from the $^5D_4$ state was monitored at 545 nm. The decay time τ_{lum} was determined according to a single-exponential law, $I_{lum}(t) = I_0\exp(-t/\tau_{lum})$.

4. Results and Discussion

4.1 Absorption

The absorption spectra of Tb^{3+} ions in KLuW are shown in Fig. 1 (for visible) and in Fig. 2 (for near-IR). The spectra are plotted for the principal light polarizations $\boldsymbol{E} \parallel N_p$, N_m and N_g. Tb:KLuW provides a strong anisotropy of the absorption spectra for polarized light which is inherent for all RE^{3+}-doped MDTs due to their low-symmetry structure. The maximum absorption corresponds to the $\boldsymbol{E} \parallel N_m$ polarization. The shape of the spectra is similar for $\boldsymbol{E} \parallel N_m$ and $\boldsymbol{E} \parallel N_g$ polarizations while being different from that for $\boldsymbol{E} \parallel N_p$. This is because for MDTs, the N_p-axis is parallel to the C_2 symmetry axis while both the N_m and N_p axes are lying in the mirror plane. Because of this, the selection rules for the 4f-4f transitions are different for light polarized along the N_p and (N_m, N_g) axes [29].

For Tb^{3+} ions, all the absorption bands at RT are due to transitions solely from the ground-state ($^7F_6$) to excited ones. This behavior is different from that for Eu^{3+} ions featuring very similar structure of the energy-levels while exhibiting transitions in absorption originating not only from the ground-state ($^7F_0$) but also from the thermally populated $^7F_1$ and even $^7F_2$ excited ones [30].

For Tb:KLuW, the weak absorption band in the visible (480-500 nm) is due to the spin-forbidden $^7F_6 \rightarrow {}^5D_4$ transition, Fig. 1(b). The maximum σ_{abs} is 3.42×10^{-21} cm^2 at 486.7 nm with a full width at half maximum (FWHM) of the corresponding absorption peak of 1.0 nm (all values are specified for $\boldsymbol{E} \parallel N_m$). The σ_{abs} is about two times lower for the light polarizations $\boldsymbol{E} \parallel N_p$ (1.73×10^{-21} cm^2 at 487.8 nm) and $\boldsymbol{E} \parallel N_g$ (1.43×10^{-21} cm^2 at 486.7 nm). The peak σ_{abs} value is higher than that for the isostructural Tb:KYbW crystal ($\sigma_{abs} = 2.3\times10^{-21}$ cm^2 at 486.7 nm) [28] and they are much higher than those for Tb^{3+}-doped fluorides, e.g., Tb:$LiLuF_4$ (0.3×10^{-21} cm^2 at 488.8 nm for π-polarization) [3]. The multiple absorption peaks at 365-385 nm are due to the spin-forbidden transitions to the higher-lying $^5D_3$, $^5G_6$ and $^5L_{10}$ excited-states, Fig. 1(a). The UV absorption edge of Tb:KLuW is at ~360 nm (E_g = 3.44 eV).

In the near-IR, Fig. 2, the absorption bands of Tb^{3+} are due to the transitions to the lower-lying $^7F_5$ – $^7F_0$ excited-states. As these transitions are spin-allowed, the peak absorption cross-sections σ_{abs} (about $2...3\times10^{-20}$ cm^2) are one order of magnitude higher than those for the absorption bands in the visible and UV ($1...2\times10^{-21}$ cm^2). The Tb:KLuW crystal is transparent until ~5.3 μm.

The spectroscopic properties of the Tb^{3+} ions were modeled within the standard Judd-Ofelt

(J-O) theory [31,32] and its modifications accounting for the configuration interaction. First, the absorption oscillator strengths for Tb^{3+} ions were determined from the measured absorption spectra as [30]:

$$\langle f_{\mathrm{exp}}^{\Sigma}\rangle(JJ') = \frac{m_e c^2}{\pi e^2 N_{\mathrm{Tb}}\langle\lambda\rangle^2}\langle\Gamma(JJ')\rangle, \tag{1}$$

where m_e and e are the electron mass and charge, respectively, c is the speed of light, ‹Γ(JJ')› is the integrated absorption coefficient and ‹λ› is the "center of gravity" of the absorption band. In the J-O modeling, we consider all the values as averaged over the three principal light polarizations, e.g., $\langle f^{\Sigma}_{\mathrm{exp}}\rangle = 1/3(f^{\Sigma}_{\mathrm{p}} + f^{\Sigma}_{\mathrm{m}} + f^{\Sigma}_{\mathrm{g}})$ [30]. The experimental $\langle f^{\Sigma}_{\mathrm{exp}}\rangle$ values are listed in Table 1. The absorption oscillator strengths were also calculated theoretically as [30]:

$$\langle f_{\mathrm{calc}}^{\Sigma}\rangle(JJ') = \frac{8}{3h(2J'+1)\langle\lambda\rangle}\frac{(\langle n\rangle^2+2)^2}{9\langle n\rangle}\langle S_{\mathrm{calc}}^{\mathrm{ED}}\rangle(JJ') + \langle f_{\mathrm{calc}}^{\mathrm{MD}}\rangle(JJ'),, \tag{2}$$

Here, h is the Planck constant and ‹n› is the mean refractive index, $\langle S^{ED}_{\mathrm{calc}}\rangle$ are the ED line strengths. The J-O theory describes electric-dipole (ED) transitions. The contribution of magnetic-dipole (MD) ones with J – J' = 0, ±1 was calculated separately within the Russell-Saunders approximation on wavefunctions of Tb^{3+} ion under the assumption of a free-ion. For the considered absorption spectrum of Tb^{3+}, these are the $^7F_6 \rightarrow {}^7F_5$ and $^7F_6 \rightarrow {}^5G_6$ transitions.

In the case of an intermediate configuration interaction (ICI), the ED line strengths are given by [33,34]:

$$\langle S_{\mathrm{calc}}^{\mathrm{ED}}\rangle(JJ') = \sum_{\mathrm{k}=2,4,6} U^{(\mathrm{k})}\tilde{\Omega}_{\mathrm{k}}\ , \tag{3}$$

where:

$$\tilde{\Omega}_{\mathrm{k}} = \Omega_{\mathrm{k}}[1 + 2R_{\mathrm{k}}(E_{\mathrm{J}} + E_{\mathrm{J'}} - 2E_{\mathrm{f}}^{0})], \tag{4a}$$

$$U^{(\mathrm{k})} = \langle(4\mathrm{f}^{\mathrm{n}})SLJ\,\|U^{\mathrm{k}}\|\,(4\mathrm{f}^{\mathrm{n}})S'L'J'\rangle^2. \tag{4b}$$

Here, $U^{(k)}$ are the squared reduced matrix elements for the transitions accounting for the absorption [28], R_k (k = 2, 4, 6) are the parameters representing the configuration interaction. In the ICI model, the J-O (intensity) parameters $\tilde{\Omega}_{\mathrm{k}}$, Eq. 4(a), are the linear functions of the energies of the two multiplets (E_J and $E_{J'}$) involved in the transition, while E_f^0 is the mean energy of the $4f^n$ configuration. In the ICI model, there are 6 free parameters, namely Ω_k and R_k (k = 2, 4, 6). If only the excited configuration with opposite parity $4f^{n-1}5d^1$ contributes to the configuration interaction, then $R_2 = R_4 = R_6 = \alpha \approx 1/(2\Delta)$ and Eq. (4a) is simplified to [33]:

$$\tilde{\Omega}_{\mathrm{k}} = \Omega_{\mathrm{k}}[1 + 2\alpha(E_{\mathrm{J}} + E_{\mathrm{J'}} - 2E_{\mathrm{f}}^{0})]. \tag{5}$$

Equation (3) with the intensity parameters given by Eq. (5) is referred as the modified J-O (mJ-O) theory. In this case, there are 4 free parameters, namely Ω_2, Ω_4, Ω_6 and α. Here, Δ means the energy of the excited configuration $4f^{n-1}5d^1$. For the case of higher-lying excited configuration of opposite parity (Δ → ∞):

$$\langle S_{\mathrm{calc}}^{\mathrm{ED}}\rangle(JJ') = \sum_{\mathrm{k}=2,4,6} U^{(\mathrm{k})}\Omega_{\mathrm{k}}. \tag{6}$$

This case corresponds to the standard J-O theory. There are three free parameters in this case, namely Ω_2, Ω_4 and Ω_6.

The calculated absorption oscillator strengths $\langle f^{ED}_{calc}\rangle$ for Tb:KLuW crystal using the J-O, mJ-O and ICI models are listed in Table 1. The ICI theory provides the smallest root mean square deviation (*rms dev.*) between the experimental, $\langle f^{\Sigma}_{exp}\rangle$, and calculated, $\langle f^{\Sigma}_{calc}\rangle = \langle f^{ED}_{calc}\rangle + \langle f^{MD}_{calc}\rangle$, absorption oscillator strengths, 0.295 (compare with rms dev. = 0.477 for the J-O theory and 0.482 for the mJ-O one). The best-fit parameters of all the used theories are listed in Table 2. In particular, for the ICI model, Ω_2 = 18.170, Ω_4 = 23.394, Ω_6 = 13.459 [10^{-20} cm^2] and R_2 = -0.102, R_4 = 0.203, R_6 = 0.170 [10^{-4} cm]. The *rms dev.* obtained in the present paper for Tb:KLuW is much lower than that reported for Tb:KYbW (0.887 with the J-O theory and 0.726 with the SCI one) [28]. This is referred mostly to the measurements of the absorption spectra in the near-IR performed in the present work, Fig. 2, where intense spin-allowed transitions $^7F_6 \rightarrow {}^7F_J$ are observed.

4.2 Emission

The probabilities for spontaneous radiative transitions are calculated from the line strengths [30]:

$$A_{\Sigma}^{calc}(JJ') = \frac{64\pi^4 e^2}{3h(2J'+1)\langle\lambda\rangle^3} n \left(\frac{n^2+2}{3}\right)^2 S_{ED}^{calc}(JJ') + A_{MD}(JJ'). \tag{7}$$

The values of $U^{(k)}$ for the transitions accounting for the emission are listed in Ref. [28]. The MD contributions were calculated in the present paper under the assumption of a free ion as described above. The mean emission wavelengths for each J → J' transition, $\langle\lambda\rangle$, were determined from the barycenters of the absorption, Fig. 1 and Fig. 2, and emission, Fig. 3, bands of Tb^{3+} ions. From the values of A for separate emission channels J → J', we calculated the total probability A^{calc}_{tot}, the radiative lifetimes of the excited-states τ_{rad} and the luminescence branching ratios for the separate emission channels B(JJ'):

$$\tau_{rad} = \frac{1}{A_{tot}^{calc}}, \text{ where } A_{tot}^{calc} = \sum_{J'} A_{\Sigma}^{calc}(JJ'), \tag{8a}$$

$$B(JJ') = \frac{A_{\Sigma}^{calc}(JJ')}{\sum_{J'} A_{\Sigma}^{calc}(JJ')} \tag{8b}$$

The results on the probabilities for radiative transitions are listed in Table 3 for transitions from the $^5D_4$ and $^5D_3$ excited states (according to the ICI theory). The radiative lifetime of the metastable $^5D_4$ state is 0.450 ms. In Table 4, we have compared the τ_{rad} values for the $^5D_4$ and $^5D_3$ states as determined with the J-O, mJ-O and SCI theories. In our previous study of an isostructural Tb:KYbW crystal [28], the $\tau_{rad}(^5D_4)$ was calculated as 2.08 ms using the strong configuration interaction (SCI) theory. This value is longer than that determined in the present work. We attribute this difference to a lower precision of the analysis in Ref. [28] due to the lack of absorption studies in the near-IR as performed in this work, cf. Fig. 2. Tb:KLuW possesses a shorter radiative lifetime of the $^5D_4$ state as compared to oxide crystals such as $TbAl_3(BO_3)_4$ ($\tau_{rad}(^5D_4)$ = 2.07 ms) [35] and $TbAlO_4$ ($\tau_{rad}(^5D_4)$ = 3.5 ms) [4].

The photoluminescence (PL) spectrum of Tb:KLuW under excitation at 488 nm (to the $^5D_4$ state) is shown in Fig. 3 for light polarization $\boldsymbol{E} \parallel N_m$. The band related to the $^5D_4 \rightarrow {}^7F_6$ transition

was measured separately under 458 nm excitation. The PL spectrum thus includes all the $^5D_4 \rightarrow {}^7F_J$ (J = 6...0) transitions: 484-500 nm (blue, J = 6), 540-552 nm (green, J = 5), 578-593 nm (orange, J = 4), 614-627 nm (red, J = 3), 639-665 nm (red, J = 2), 665-685 nm (deep-red, J = 1) and 686-700 nm (deep-red, J = 0). The corresponding emission colors are indicated in Fig. 3 by filling the spectra. The most intense emission band is due to the $^5D_4 \rightarrow {}^7F_5$ transition that is typical for Tb^{3+}-doped materials [4].

The scheme of energy-levels of Tb^{3+} ions and the observed transitions in absorption and emission are shown in Fig. 4. In this figure, we have also indicated the efficient resonant cross-relaxation (CR) process, $^5D_3 + {}^7F_6 \rightarrow {}^5D_4 + {}^7F_{0,1}$, responsible for the depopulation of the $^5D_3$ excited-state [36].

The measured PL decay curves for Tb^{3+} ions in a 3 at.% Tb:KLuW crystal are plotted in Fig. 5. The emission was monitored at 545 nm (from the $^5D_4$ state). Several excitation wavelengths were tested, namely 475 nm (direct excitation to the emitting state), 380 nm (to the $^5D_3$ excited-state) and 365 nm (to the higher-lying $^5L_{10}$ one). All the measured curves are clearly single-exponential as revealed in Fig. 5 plotted in a semi-log scale. This agrees with the accommodation of Tb^{3+} ions in a single type of site (Lu^{3+} site with a C_2 symmetry and VIII-fold O^{2-} coordination [21], ionic radii: 0.977 Å for Lu^{3+} and 1.04 Å for Tb^{3+}). The luminescence decay time τ_{lum} is 411±3 μs. The τ_{lum} is slightly shorter than the radiative one, resulting in a luminescence quantum efficiency $\eta_q = \tau_{lum}/\tau_{rad}$ of 91%. Such a high value can be expected for Tb^{3+} ions due to the large energy gap between the $^5D_4$ state and the lower-lying excited-state ($^7F_0$) which is about 15000 cm^{-1} [2]. Indeed, as the maximum phonon frequency $h\nu_{max}$ of KLuW is 908 cm^{-1} [21], the non-radiative relaxation from the $^5D_4$ state is not probable. A similar effect is observed for the metastable $^5D_0$ state of Eu^{3+} ions in KLuW [30]. Previously for the isostructural 1 at.% Tb:KYbW and 5 at.% Tb:KYW crystals, $\tau_{lum}(^5D_4)$ was determined to be 395 μs and 460 μs, respectively, which is close to the value measured in the present work [26,28].

The PL spectra of Tb^{3+} ions were measured for all three principal light polarizations, $\boldsymbol{E} \parallel N_p$, N_m and N_g. Using such spectra, the polarized stimulated-emission (SE) cross-section, σ_{SE}, spectra for Tb^{3+} ions were calculated with the Füchtbauer–Ladenburg (F-L) equation [37]:

$$\sigma_{SE}^{i}(\lambda) = \frac{\lambda^5}{8\pi n_i^2 \tau_{rad} c} \frac{W_i(\lambda) B(\mathrm{JJ'})}{1/3 \sum_{i=p,m,g} \int \lambda W_i(\lambda) \mathrm{d}\lambda}. \tag{9}$$

Here, $W_i(\lambda)$ is the measured spectral power density of luminescence for the i-th polarization, $i = p, m, g$, n_i is the corresponding refractive index taken from [21], τ_{rad} is the radiative lifetime of the $^5D_4$ state of Tb^{3+} and integration in Eq. (9) is performed within the emission band corresponding to the particular $^5D_4 \rightarrow {}^7F_J$ transition. The σ_{SE} spectra are shown in Fig. 6. The Tb^{3+} ions in KLuW exhibit strong anisotropy for polarized light. The maximum σ_{SE} values correspond to $\boldsymbol{E} \parallel N_m$ (so that this polarization is the most attractive for laser operation), the intermediate ones – to $\boldsymbol{E} \parallel N_p$ and the lowest ones – to light polarized parallel to the N_g-axis. This trend is similar for most of the RE^{3+} ions in MDTs [21]. For the $^5D_4 \rightarrow {}^7F_5$ transition, the maximum $\sigma_{SE} = 11.4\times10^{-21}$ cm^2 at 549.4 nm (for $\boldsymbol{E} \parallel N_m$). The peak σ_{SE} values for all the $^5D_4 \rightarrow {}^7F_J$ transitions are listed in Table 5. The maximum σ_{SE} value for Tb^{3+} ions in KLuW is much larger than those for $Tb:LiLuF_4$ crystal, namely ~1.6×10^{-21} cm^2 at ~540 nm for σ-polarization [3].

The unpolarized PL spectra of the Tb:KLuW crystal under blue excitation were characterized in terms of the CIE 1931 (*Commission internationale de l'éclairage*) chromaticity diagram. The color coordinates are x = 0.380 and y = 0.608 that fall into the yellowish green region. The dominant wavelength λ_d is 561 nm with a color purity p of >97% (for a 2 degree observer).

5. Conclusion

The Tb^{3+}-doped monoclinic $KLu(WO_4)_2$ crystal is promising for color tunable visible (green and yellow) lasers. Due to its low-symmetry structure, it features high transition cross-sections for absorption and emission with polarized light. The upper-laser level ($^5D_4$) lifetime of Tb^{3+} ions is 411 μs (for 3 at.% Tb^{3+} doping) and the luminescence quantum yield is >90%. We have successfully applied the J-O theory modified for the case of an intermediate configuration interaction (ICI) for the description of the transition probabilities of Tb^{3+} ions in $KLu(WO_4)_2$. Due to the measurements of the characteristic Tb^{3+} absorption ($^7F_6 \rightarrow {}^7F_J$, J = 0...5) in the near- and mid-IR, we were able to improve the quality of the J-O analysis and to predict a higher luminescence quantum efficiency of Tb^{3+}:$KLu(WO_4)_2$ crystals, similarly to those doped with Eu^{3+} ions. We determine that $KLu(WO_4)_2$ doped with Tb^{3+} is more attractive than the isostructural stoichiometric crystal Tb^{3+}:$KYb(WO_4)_2$ studied recently due to the higher transition cross-sections and the lack of parasitic cooperative $2Yb^{3+} \leftrightarrow Tb^{3+}$ processes.

As the transitions suitable for Tb^{3+} pumping (e.g., $^7F_6 \rightarrow {}^5D_4$, falling in the blue spectral range) are spin-forbidden, relatively high doping concentrations of Tb^{3+} are required to ensure high pump absorption efficiency. The future work will focus on the growth of highly Tb^{3+}-doped $KLu(WO_4)_2$ crystals (the isostructural series of monoclinic $KLu_{1-x}Tb_x(WO_4)_2$ up to the stoichiometric $KTb(WO_4)_2$ exists) and the study of the concentration effects on the Tb^{3+} spectroscopy, e.g., the luminescence quenching and the cross-relaxation. The study of an excited-state absorption of Tb^{3+} in $KLu(WO_4)_2$ (from the $^5D_4$ state) to the higher-lying excited states of the $4f^8$ configuration and to the ^9D and ^7D states of the excited $4f^75d^1$ configuration is also relevant for obtaining lasing in the Tb^{3+} ions.

Acknowledgements

This work was supported by the Spanish Government under projects MAT2016-75716-C2-1-R (AEI/FEDER,UE) and TEC2014-55948-R, and by the Generalitat de Catalunya under project 2014SGR1358. F.D. acknowledges additional support through the ICREA academia award 2010ICREA-02 for excellence in research. P.L. acknowledges financial support from the Government of the Russian Federation (Grant 074-U01) through ITMO Post-Doctoral Fellowship scheme.

References

1. C. Kränkel, D.-T. Marzahl, F. Moglia, G. Huber, P.W. Metz, Out of the blue: semiconductor laser pumped visible rare-earth doped lasers, Laser Photon. Rev. 10 (2016) 548–568.
2. W.T. Carnall, P.R. Fields, K. Rajnak, Electronic energy levels of the trivalent lanthanide aquo ions. III. Tb^{3+}, J. Chem. Phys. 49 (1968) 4447-4449.

3. P.W. Metz, D.-T. Marzahl, A. Majid, C. Kränkel, G. Huber, Efficient continuous wave laser operation of Tb^{3+}-doped fluoride crystals in the green and yellow spectral regions, Laser Photon. Rev. 10 (2016) 335–344.
4. D.K. Sardar, K.L. Nash, R.M. Yow, J.B. Gruber, U.V. Valiev, E.P. Kokanyan, Absorption intensities and emission cross sections of $Tb^{3+}(4f^8)$ in $TbAlO_3$, J. Appl. Phys. 100 (2006) 083108-1-5.
5. T. Hayakawa, N. Kamata, and K. Yamada, Visible emission characteristics in Tb^{3+}-doped fluorescent glasses under selective excitation, J. Lumin. 68 (1996) 179-186.
6. X. Y. Sun, M. Gu, S. M. Huang, X. J. Jin, X. L. Liu, B. Liu, C. Ni, Luminescence behavior of Tb^{3+} ions in transparent glass and glass-ceramics containing CaF_2 nanocrystals, J. Lumin. 129 (2009) 773-777.
7. G. Lakshminarayana, J. Qiu, M.G. Brik, I.V. Kityk, Photoluminescence of Eu^{3+}-, Tb^{3+}-, Dy^{3+}-and Tm^{3+}-doped transparent GeO_2–TiO_2–K_2O glass ceramics, J. Phys. Condens. Matter 20 (2008) 335106-1-11.
8. X. Ju, X. Li, W. Li, W. Yang, C. Tao, Luminescence properties of $ZnMoO_4$:Tb^{3+} green phosphor prepared via co-precipitation, Mater. Lett. 65 (2011) 2642–2644.
9. J. Liao, B. Qiu, H. Lai, Synthesis and luminescence properties of Tb^{3+}:$NaGd(WO_4)_2$ novel green phosphors, J. Lumin. 129 (2009) 668–671.
10. Z. Hao, J. Zhang, X. Zhang, S. Lu, X. Wang, Blue-green-emitting phosphor $CaSc_2O_4$:Tb^{3+}: tunable luminescence manipulated by cross-relaxation, J. Electrochem. Soc. 156 (2009) H193-H196.
11. S. Som, S.K. Sharma, Eu^{3+}/Tb^{3+}-codoped Y_2O_3 nanophosphors: Rietveld refinement, bandgap and photoluminescence optimization, J. Phys. D 45 (2012) 415102-1-11.
12. M. Xu, L. Wang, D. Jia, H. Zhao, Tuning the color emission of $Sr_2P_2O_7$:Tb^{3+},Eu^{3+} phosphors based on energy transfer, J. Am. Ceram. Soc. 98 (2015) 1536-1541.
13. P. Vergeer, T.J. Vlugt, M.H. Kox, M.I. Den Hertog, J.P. Van der Eerden, A. Meijerink, Quantum cutting by cooperative energy transfer in $Yb_xY_{1-x}PO_4$:Tb^{3+}, Phys. Rev. B 71 (2005) 014119-1-11.
14. J.L. Yuan, X.Y. Zeng, J.T. Zhao, Z.J. Zhang, H.H. Chen, X.X. Yang, Energy transfer mechanisms in Tb^{3+},Yb^{3+} codoped Y_2O_3 downconversion phosphor, J. Phys. D 41 (2008) 105406-1-6.
15. S.I. Andreev, M.R. Bedilov, G.O. Karapetyan, V. M. Likhachev, Stimulated emission of glass activated by terbium, Sov. J. Opt. Technol. 34 (1967) 819.
16. S. Bjorklund, G. Kellermeyer, C.R. Hurt, N. McAvoy, N. Filipescu, Laser action from terbium trifluoroacetylacetonate in *p*-dioxane and acetonitrile at room temperature, Appl. Phys. Lett. 10 (1967) 160-162.
17. H.P. Jenssen, D. Castleberry, D. Gabbe, and A. Linz, Stimulated emission at 5445 Å in Tb^{3+}:YLF, IEEE J. Quantum Electron. 9 (1973) 665.
18. T. Yamashita Y. Ohishi, Amplification and lasing characteristics of Tb^{3+}-doped fluoride fiber in the 0.54 µm band, Jpn. J. Appl. Phys. 46 (2007) L991-L993.
19. P.W. Metz, D.T. Marzahl, G. Huber, C. Kränkel, Performance and wavelength tuning of green emitting terbium lasers, Opt. Express 25 (2017) 5716-5724.
20. P. Dorenbos, The 5d level positions of the trivalent lanthanides in inorganic compounds, J. Lumin 91 (2000) 155-176.
21. V. Petrov, M.C. Pujol, X. Mateos, Ò. Silvestre, S. Rivier, M. Aguiló, R.M. Solé, J. Liu, U. Griebner, F. Díaz, Growth and properties of $KLu(WO_4)_2$, and novel ytterbium and thulium lasers based on this monoclinic crystalline host, Laser & Photon. Rev. 1 (2007) 179–212.

22. P.A. Loiko, V.I. Dashkevich, S.N. Bagaev, V.A. Orlovich, A.S. Yasukevich, K.V. Yumashev, N.V. Kuleshov, E.B. Dunina, A.A. Kornienko, S.M. Vatnik, A.A. Pavlyuk, Spectroscopic characterization and pulsed laser operation of Eu^{3+}:$KGd(WO_4)_2$ crystal, Laser Phys. 23 (2013) 105811-1-7.
23. V.I. Dashkevich, S.N. Bagayev, V.A. Orlovich, A.A. Bui, P.A. Loiko, K.V. Yumashev, N.V. Kuleshov, S.M. Vatnik, A.A. Pavlyuk, Quasi-continuous wave and continuous wave laser operation of Eu:$KGd(WO_4)_2$ crystal on a $^5D_0 \rightarrow {}^7F_4$ transition, Laser Phys. Lett. 12 (2014) 015006-1-6.
24. A.A. Kaminskii, J.B. Gruber, S.N. Bagaev, K.I. Ueda, U. Hömmerich, J.T. Seo, D. Temple, B. Zandi, A.A. Kornienko, E.B. Dunina, A.A. Pavlyuk, Optical spectroscopy and visible stimulated emission of Dy^{3+} ions in monoclinic α-$KY(WO_4)_2$ and α-$KGd(WO_4)_2$ crystals, Phys. Rev. B 65 (2002) 125108-1-29.
25. H. Zhao, J. Wang, J. Li, H. Zhang, J. Zhang, Z. Ling, H. Xia, R.I. Boughton, Optical and thermal properties of crystalline Tb:$KLu(WO_4)_2$, Mater. Lett. 61 (2007) 2499–2501.
26. S. Schwung, D. Rytz, B. Heying, U.Ch. Rodewald, O. Niehaus, D. Enseling, T. Jüstel, R. Pöttgen, The crystal structure and luminescence quenching of poly-and single-crystalline KYW_2O_8:Tb^{3+}, J. Lumin. 166 (2015) 289-294.
27. W. Strek, P.J. Deren, A. Bednarkiewicz, Cooperative processes in $KYb(WO_4)_2$ crystal doped with Eu^{3+} and Tb^{3+} ions, J. Lumin. 87–89 (2000) 999–1001.
28. P. Loiko, X. Mateos, E. Dunina, A. Kornienko, A. Volokitina, E. Vilejshikova, J.M. Serres, A. Baranov, K. Yumashev, M. Aguiló, F. Díaz, Judd-Ofelt modelling and stimulated-emission cross-sections for Tb^{3+} ions in monoclinic $KYb(WO_4)_2$ crystal, J. Lumin. 190 (2017) 37-44.
29. P.A. Loiko, E.V. Vilejshikova, X. Mateos, J.M. Serres, E.B. Dunina, A.A. Kornienko, K.V. Yumashev, M. Aguiló, F. Díaz, Europium doping in monoclinic $KYb(WO_4)_2$ crystal, J. Lumin. 183 (2017) 217-225.
30. P.A. Loiko, V.I. Dashkevich, S.N. Bagaev, V.A. Orlovich, A.S. Yasukevich, K.V. Yumashev, N.V. Kuleshov, E.B. Dunina, A.A. Kornienko, S.M. Vatnik, A.A. Pavlyuk, Spectroscopic and photoluminescence characterization of Eu^{3+}-doped monoclinic $KY(WO_4)_2$ crystal, J. Lumin. 153 (2014) 221-226.
31. B.R. Judd, Optical absorption intensities of rare-earth ions, Phys. Rev. 172 (1962) 750–761.
32. G.S. Ofelt, Intensities of crystal spectra of rare-earth ions, J. Chem. Phys. 37 (1962) 511–519.
33. A.A. Kornienko, A.A. Kaminskii, E.B. Dunina, Dependence of the line strength of f–f transitions on the manifold energy. II. Analysis of Pr^{3+} in $KPrP_4O_{12}$, Phys. Stat. Sol. (b) 157 (1990) 267-273.
34. P.A. Loiko, A.S. Yasukevich, A.E. Gulevich, M.P. Demesh, M.B. Kosmyna, B.P. Nazarenko, V.M. Puzikov, A.N. Shekhovtsov, A.A. Kornienko, E.B. Dunina, N.V. Kuleshov, Growth, spectroscopic and thermal properties of Nd-doped disordered $Ca_9(La/Y)(VO_4)_7$ and $Ca_{10}(Li/K)(VO_4)_7$ crystals, J. Lumin. 137 (2013) 252-258.
35. S. Colak, W.K. Zwicker, Transition rates of Tb^{3+} in TbP_5O_{14}, $TbLiP_4O_{12}$, and $TbAl_3(BO_3)_4$: An evaluation for laser applications, J. Appl. Phys. 54 (1983) 2156-2166.
36. D.J. Robbins, B. Cockayne, B. Lent, J.L. Glasper, The mechanism of $^5D_3 - {}^5D_4$ cross-relaxation in $Y_3Al_5O_{12}$:Tb^{3+}, Solid State Commun. 20 (1976) 673-676.
37. B.F. Aull, H.P. Jenssen, Vibronic interactions in Nd:YAG resulting in nonreciprocity of absorption and stimulated emission cross sections, IEEE J. Quantum Electron. 18 (1982) 925–930.

Table 1. Experimental and calculated absorption oscillator strengths for a 3 at.% Tb:KLuW crystal.

Transition	f^{Σ}_{exp}, 10^{-6}			$\langle f^{\Sigma}_{exp}\rangle$*,	$\langle f^{ED}_{calc}\rangle$*, 10^{-6}			$\langle f^{MD}_{calc}\rangle$
	N_p	N_m	N_g	10^{-6}	J-O	mJ-O	ICI	
$^7F_6 \rightarrow {}^7F_5$	7.20	9.45	4.26	6.97	6.38^{ED}	6.27^{ED}	6.33^{ED}	0.57^{MD}
$^7F_6 \rightarrow {}^7F_4$	4.97	5.04	2.15	4.06	4.32^{ED}	4.38^{ED}	4.28^{ED}	-
$^7F_6 \rightarrow {}^7F_3$	4.33	3.60	2.97	3.63	3.27^{ED}	3.22^{ED}	3.32^{ED}	-
$^7F_6 \rightarrow {}^7F_{1,2}$	4.98	6.22	3.24	4.81	4.98^{ED}	4.95^{ED}	4.89^{ED}	-
$^7F_6 \rightarrow {}^7F_0$	0.96	1.07	0.45	0.83	0.86^{ED}	0.85^{ED}	0.85^{ED}	-
$^7F_6 \rightarrow {}^5D_4$	0.34	0.59	0.16	0.36	0.20^{ED}	0.22^{ED}	0.24^{ED}	-
$^7F_6 \rightarrow {}^5D_3 + {}^5G_6$	1.42	2.70	1.25	1.79	0.64^{ED}	0.76^{ED}	1.55^{ED}	0.21^{MD}
rms dev.					*0.477*	*0.482*	*0.295*	

*f^{Σ}_{exp} - experimental oscillator strengths, polarization-averaging: $\langle f^{\Sigma}_{exp}\rangle = 1/3(f^{\Sigma}_{p} + f^{\Sigma}_{m} + f^{\Sigma}_{g})$, $\langle f_{calc}\rangle$ - calculated ones (ED and MD stand for electric and magnetic dipole contributions, respectively), *rms dev.* - root-mean-square deviation between $\langle f^{\Sigma}_{exp}\rangle$ and $\langle f^{\Sigma}_{calc}\rangle = \langle f^{ED}_{calc}\rangle + \langle f^{MD}_{calc}\rangle$.

Table 2. Parameters of J-O, mJ-O and ICI theories applied to calculate the absorption oscillator strengths for a Tb:KLuW crystal.

Theory	Parameters	Value: Tb:KLuW
J-O	Ω_k [10^{-20} cm^2]	Ω_2 = 23.524, Ω_4 = 8.111, Ω_6 = 6.918
mJ-O	Ω_k [10^{-20} cm^2];	Ω_2 = 25.496, Ω_4 = 9.590, Ω_6 = 7.589;
	α [10^{-4} cm]	α = 0.033
ICI	Ω_k [10^{-20} cm^2];	Ω_2 = 18.170, Ω_4 = 23.394, Ω_6 = 13.459;
	R_k [10^{-4} cm]	R_2 = -0.102, R_4 = 0.203, R_6 = 0.170

Table 3. Calculated emission probabilities for Tb^{3+} ions in a 3 at.% Tb:KLuW crystal (for the ICI theory).

Excited state	Terminating state	$A_{JJ'}$, s^{-1}	$B_{JJ'}$, %	A_{tot}, s^{-1}	τ_{rad}, ms
$^5D_4\rightarrow$	$^7F_6$	351.4^{ED}	15.8	2221.6	0.450
	$^7F_5$	$1076.6^{ED}+90.5^{MD}$	52.5		
	$^7F_4$	$241.3^{ED}+0.4^{MD}$	10.9		
	$^7F_3$	$139.5^{ED}+10.8^{MD}$	6.8		
	$^7F_2$	65.5^{ED}	2.9		
	$^7F_1$	148.7^{ED}	6.7		
	$^7F_0$	97.9^{ED}	4.4		
$^5D_3\rightarrow$	$^7F_6$	383.2^{ED}	8.5	4535.0	0.221
	$^7F_5$	1227.5^{ED}	27.1		
	$^7F_4$	$916.9^{ED}+105.2^{MD}$	22.5		
	$^7F_3$	$340.2^{ED}+1.6^{MD}$	7.5		
	$^7F_2$	$772.2^{ED}+30.4^{MD}$	17.7		
	$^7F_1$	413.6^{ED}	9.1		
	$^7F_0$	--	-		
	$^5D_4$	$294.5^{ED}+49.7^{MD}$	7.6		

$A_{JJ'}$ - probability of spontaneous transition (ED and MD stand for electric and magnetic dipole contributions, respectively), $B_{JJ'}$ - luminescence branching ratio, A_{tot} - total probability of spontaneous transitions, τ_{rad} – radiative lifetime.

Table 4. Calculated radiative lifetimes of the $^5D_4$ and $^5D_3$ excited-states of Tb^{3+} ions in KLuW crystal (for J-O, mJ-O and ICI theories).

Excited state	τ_{rad}, ms		
	J-O	mJ-O	ICI
$^5D_4$	0.500	0.449	0.450
$^5D_3$	0.323	0.275	0.221

Table 5. Peak stimulated-emission cross-sections for $\boldsymbol{E} \parallel N_m$, σ_{SE}, for Tb^{3+} ions in KLuW crystal, as calculated with the F-L formula using the luminescence branching ratios from Table 4).

Transition	σ_{SE}, 10^{-21} cm^2	λ_{peak}, nm	Color
$^5D_4 \rightarrow {}^7F_6$	1.15	487.9	blue
$^5D_4 \rightarrow {}^7F_5$	11.4	549.4	green
$^5D_4 \rightarrow {}^7F_4$	2.29	590.9	orange
$^5D_4 \rightarrow {}^7F_3$	1.75	625.0	red
$^5D_4 \rightarrow {}^7F_2$	1.84	652.5	red
$^5D_4 \rightarrow {}^7F_1$	1.88	670.6	deep-red
$^5D_4 \rightarrow {}^7F_0$	0.23	688.4	deep-red

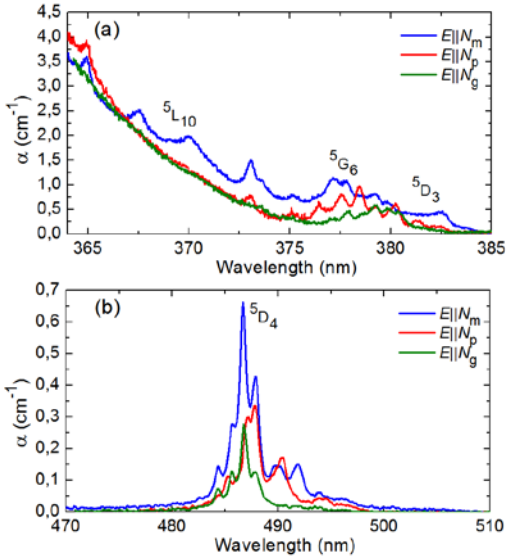

Figure 1. Visible absorption spectra of a 3 at.% Tb:KLuW crystal with polarized light at RT: Transitions $^7F_6 \rightarrow {}^5D_3$, $^5G_6$, $^5L_{10}$ (a) and $^7F_6 \rightarrow {}^5D_4$ (b).

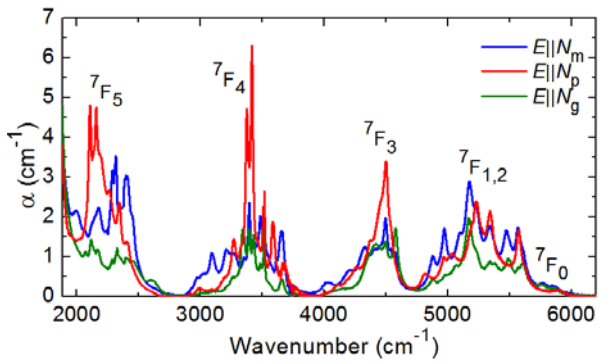

Figure 2. Near-IR absorption spectra of a 3 at.% Tb:KLuW crystal with polarized light at RT.

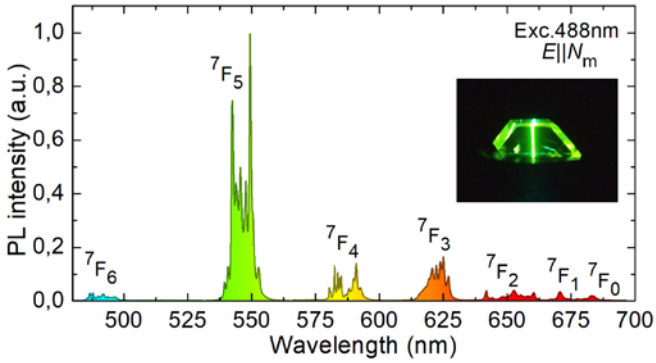

Figure 3. Combined photoluminescence (PL) spectrum of a 3 at.% Tb:KLuW crystal at RT for light polarization $\boldsymbol{E} \parallel N_m$; the excitation wavelength is 458 nm ($^5D_4 \rightarrow {}^7F_6$ emission band) and 488 nm (remaining bands). The color fill corresponds to the emission wavelength. *Inset* shows a photo of the crystal under excitation.

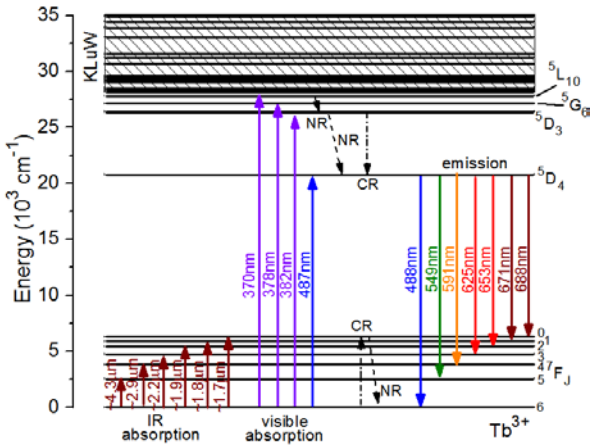

Figure 4. Scheme of the energy levels of Tb^{3+} ions in KLuW and the observed transitions for absorption and emission (shown by *solid arrows*). NR – non-radiative relaxation, CR – cross-relaxation. Dashed area – host absorption of KLuW.

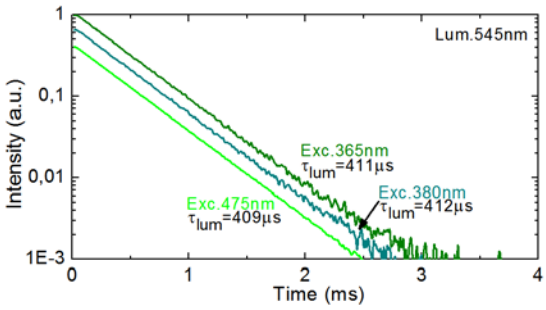

Figure 5. Decay of the green luminescence of Tb^{3+} ions at 545 nm for a 3 at.% Tb:KLuW crystal at RT, the excitation wavelength is 365 nm, 380 nm or 475 nm, τ_{lum} is the luminescence decay time according to a single-exponential fit.

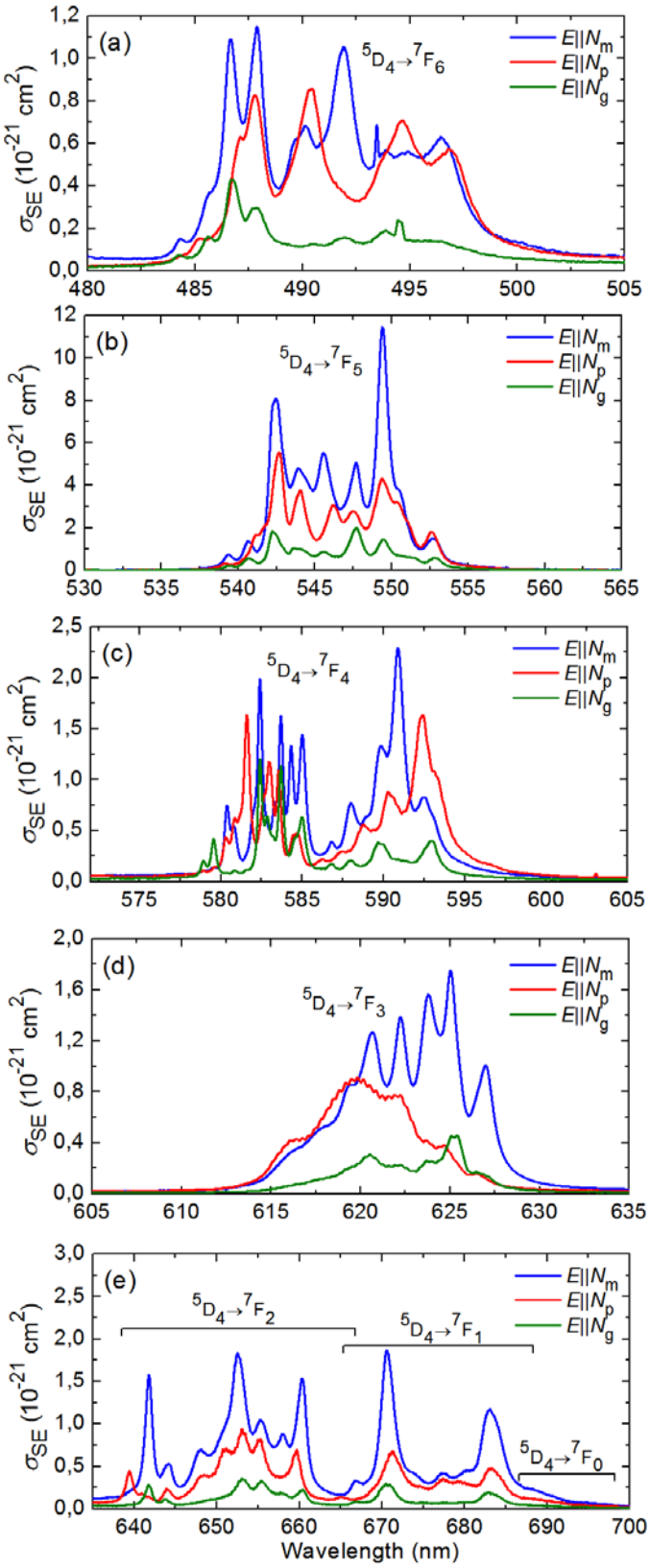

Figure 6. (a)-(e) Stimulated-emission cross-sections, σ_{SE}, for Tb^{3+} ions in KLuW crystal at RT (for the principal light polarizations, $\boldsymbol{E} \parallel N_p$, N_m and N_g, as calculated with the F-L formula using the luminescence branching ratios from Table 4).